Unsteady numerical analysis of drag on non-winged hypersonic vehicle during re-entry

IOP Conf. Series: Materials Science and Engineering **610** (2019) 012096 doi:10.1088/1757-899X/610/1/012096

Unsteady numerical analysis of drag on non-winged hypersonic vehicle during re-entry

Mohamed S Abdel-Gawad[1], Mostafa S Khalil[1] and Mahmoud Y M Ahmed[1]

[1]Aerospace Engineering Department, Military Technical College, Cairo, Egypt

E-mail: mohamed.saied.abdelgawad@gmail.com

Abstract. Reentry vehicles, such as upper stages of ballistic missiles, experience severe aerodynamic loads during the reentry phase of trajectory. This phase is characterized by three aspects namely, the continuous change in atmospheric conditions, the hypersonic flight speed, and the unsteady flight of the vehicle itself. Understanding the aerodynamic features of the vehicle during reentry phase is crucial to the designers of such vehicles. The objective of the present study is to investigate the aerodynamic features of a generic bi-cone non-winged vehicle that accelerates during reentry through the upper layer of dense atmosphere. The investigation is conducted via numerically simulating the unsteady flow around the vehicle using a commercial transient laminar CFD solver. The unsteady simulation accounts for the temporal variation of freestream conditions and the linear acceleration of the vehicle during descent. The used CFD model is validated against available wind tunnel data of a similar vehicle. The results address the evolution of the flow field pattern as well as the temporal variation of drag acting on the vehicle during reentry.

Keywords: Reentry vehicle, Hypersonic aerodynamics, CFD, Unsteady aerodynamics.

1. Introduction

After the Second World War, particularly during the fifties and sixties of the 20th century, space discovery started to be a point of interest for scientists who worked on sending man into space and orbits around Earth using rockets. Their biggest obstacle was finding out how to bring back space vehicles to Earth safely. Thus, the design of such re-entry vehicles emerged, as well as understanding the phenomena taking place during their hypersonic flight.

The term “re-entry” emphasizes the fact that such vehicles exit the dense layers of atmosphere and return back to Earth; i.e., re-enter the atmosphere, during decent. Multistage ballistic missiles are designed to deliver their payload, the upper stage, at relatively long ranges. Upper stages of ballistic missiles are, by definition, re-entry vehicles as well.

The complexities of phenomena around the re-entry vehicles during descent phase stem from the continuous and sharp variation in properties of the surrounding air. Basically, air pressure increases during descent as well as density while temperature changes in different patterns according to the atmospheric layer. Hence, the type of flow around the vehicle changes from free molecular, to slip flow, and eventually to continuum flow (at altitude less than 90 km) as the value of Knudsen number changes [1, 2]. In addition, the re-entry vehicle itself experiences variation in velocity during descent under the action of gravity along with pitching unsteadiness. Finally, the flow field around reentry vehicles is hypersonic (flight Mach number higher than 5) that includes the effects of the high temperature gas, energy flux, strong shock waves, and shock-boundary layer interaction.

Numerical simulation based on CFD technique is a suitable alternative to investigate the phenomena taking place during the flight of reentry vehicles. This is because of the unavailability or high cost of wind tunnel experiments and the flight tests. Numerical simulation tools based on Navier-Stokes equations assume that the flow around the vehicle is a continuum flow of real gas. This condition approximately applies for flight altitudes below 90 Km in standard atmosphere [3].

In the open literature, few studies on flow unsteadiness around hypersonic reentry vehicles can be found. Weiland [4] reported a comprehensive database on a wide variety of reentry vehicles and their aerodynamic characteristics. However, only steady values were reported, unsteady characteristics of these vehicles were not available. In contrast, investigating unsteady aerodynamic features around complete missile and projectile configurations at supersonic and low hypersonic speeds are more available in the open literature. For instance, Sahu [5] conducted numerical simulation of unsteady aerodynamics for spinning finned projectile at supersonic speed equals to 1037 m/s with spin rate equal to 2500 rad/s during free flight whereas unsteadiness was in the form of spinning. Similarly, Cayzac et al. [6] computed unsteady aerodynamic coefficients for a model of a fin-stabilized projectile. Focus was made on yawing-spinning motion; results were compared with wind tunnel measurements. Wind tunnel test conditions corresponded to freesream Mach numbers of 2.89 and 4.49 at a constant altitude. Gledhill et al. [7] investigated the longitudinal acceleration effects on missile aerodynamics using CFD at acceleration equals to 4500 m/s^2 in freestream speed of Mach range from 1 to 5. Variation of drag coefficient with Mach number was briefly reported. The calculated drag coefficient was normalized with respect to instantaneous dynamic pressure.

The apparent shortage in open studies on unsteady aerodynamics of reentry vehicles at hypersonic flight conditions and varying flight altitudes is the prime motivation of the present research. To partially fulfil this research, the objective of the present paper is to simulate the hypersonic flow around a generic model representing the upper stage of a ballistic missile during real descent accelerating from 87 km to 77 km for a duration of ten seconds. The freestream conditions are defined to represent the variation in vehicle speed as well as atmospheric properties. Focus is made on understanding the temporal variation in drag during this phase. The evolution of flow field structure around the vehicle during descent is also discussed. A commercial CFD tool is utilized in the study.

The remainder of this paper is organized as follows, the case study and study approach are explained next, the key findings are represented and discussed, the paper finalizes with the main conclusions.

2. Case Study and Methodology

A generic model representing the upper stage of a ballistic missile is considered. It has the form of a bicone with a fineness ratio of 2.5 with a multi-step tip. The three dimensional model configuration is shown in the figure below.

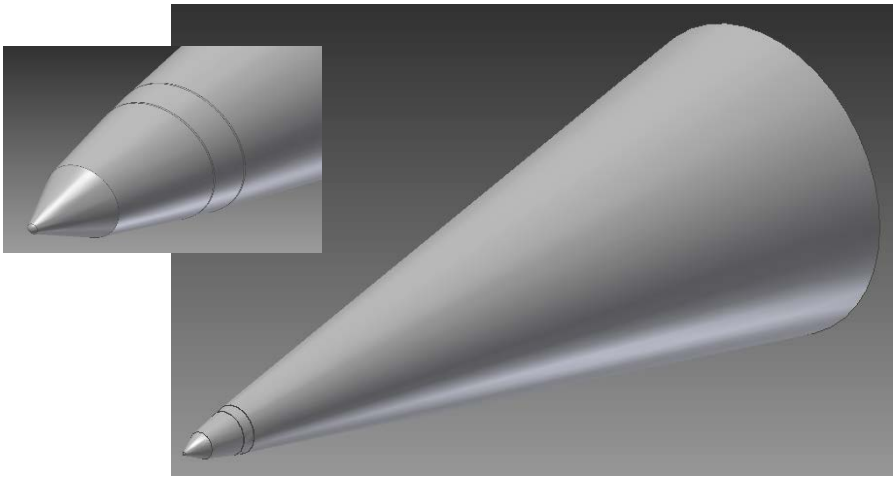

Figure 1. Configuration of the case study model

A computational domain is built depending on the range of Mach no. in concern; the key aspect for setting the domain dimensions. Thus, the domain dimensions are chosen to ensure that all flow field features generated around the model are enclosed by the domain. The figure below shows the domain dimensions relative to the full model length (L). The boundary definitions used in the simulation are also shown in the figure. 2.
Since the vehicle and the flow are symmetric and only longitudinal acceleration is considered, an axisymmetric domain is utilized rather than a three-dimensional domain to minimize the simulation budget.

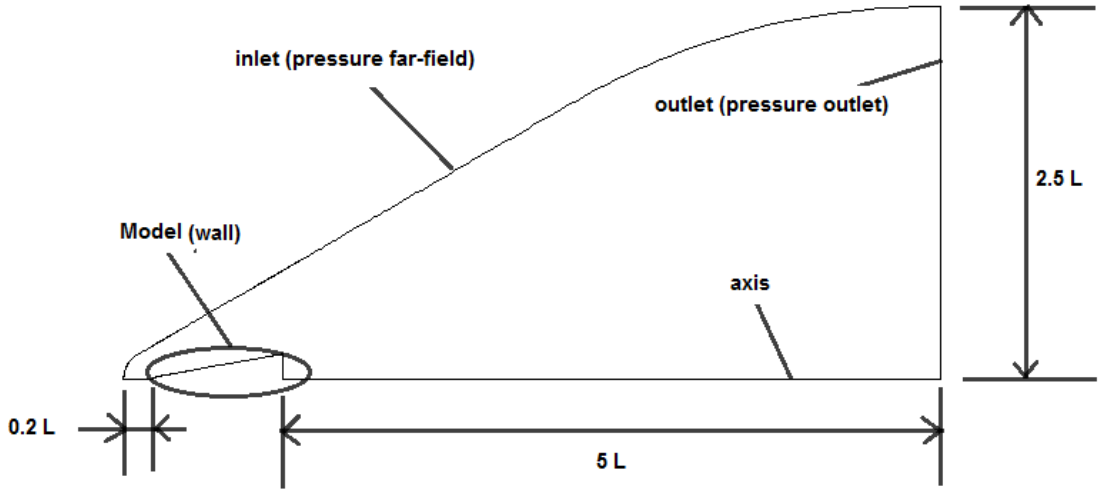

Figure 2. Shape, extents, and boundary definitions of the computational domain

The domain is divided into eight blocks at each discontinuity on the model contour to generate a structured grid. The set of figures below shows the discretized domain as well as a zoom in on the model.

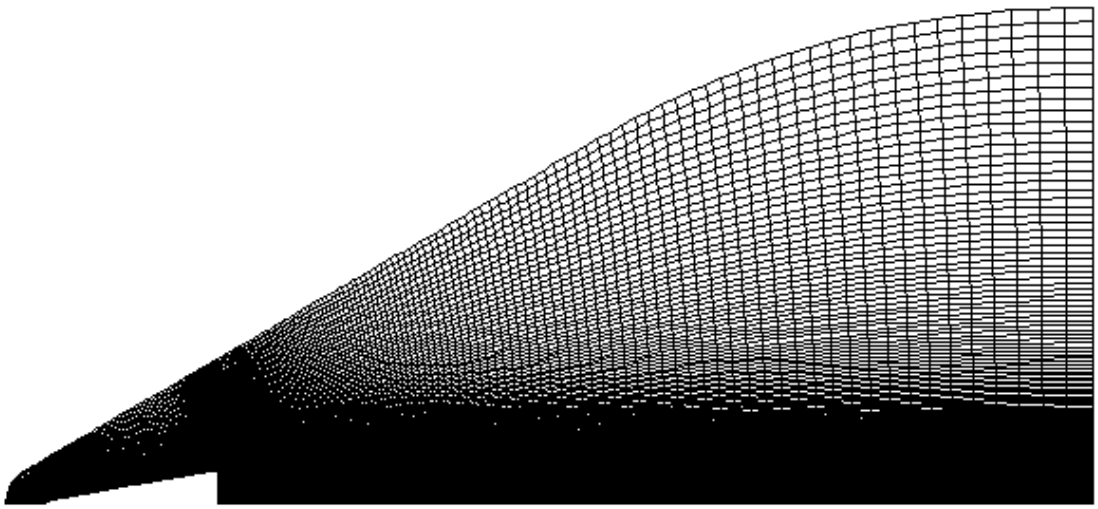

(a)

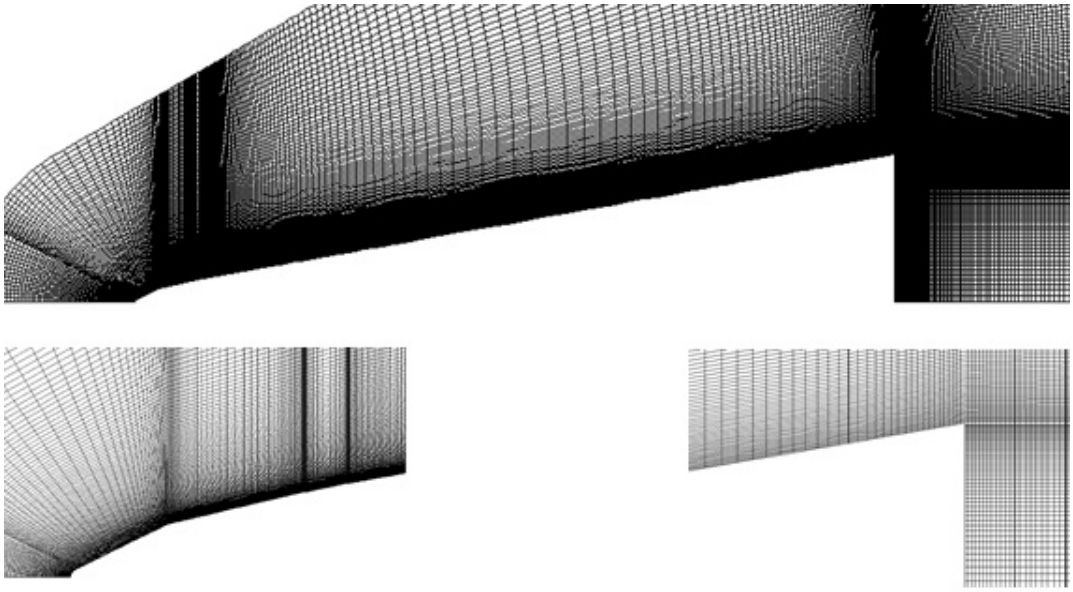

(b)

Figure 3. Features of the (a) full discretized domain and (b) zoom-in views

A grid sensitivity check is conducted for four grid resolutions to obtain the grid-independent solution. In the sensitivity check, the boundary condition represents a Mach 6 flow at standard sea level conditions and the total drag coefficient is taken as a measure for solution quality. Table 1 lists the results of the grid sensitivity check. Improvement in drag coefficient value using grid 4 is insignificant. Hence, grid 3 is adopted in the present study.

Table 1. Results of the grid sensitivity check

Grid	No. of cells	First cell height	C_D	%improvement
1	2900	23 mm	0.1384	----------
2	13200	0.5 mm	0.1236	10.69
3	91100	0.15 mm	0.1226	0.81
4	360200	0.007 mm	0.1225	0.08

The freestream flow properties vary during accelerating descent of the vehicle. These properties are calculated by solving the flight trajectory problem. A computer code is developed based on 3-degree of freedom flight model equations to simulate the flight from the point of separation till ground impact. Flight altitude, speed, and path angle at separation are 39 km, 2020 m/s, and 40^0, respectively [8].

According to the flight simulation results, the temporal variation of flight altitude and velocity during the descent phase in concern (below 87 km for 10 seconds) is illustrated in figure 4a below while figure 4 b and c show the temporal variation of freestream flow properties during the same phase in a standard atmosphere [9]. The freestream Reynolds number is calculated based on the vehicle base diameter. For the range of altitudes in concern, the Knudsen number is found to be below 0.01; a continuum assumption is considered valid.

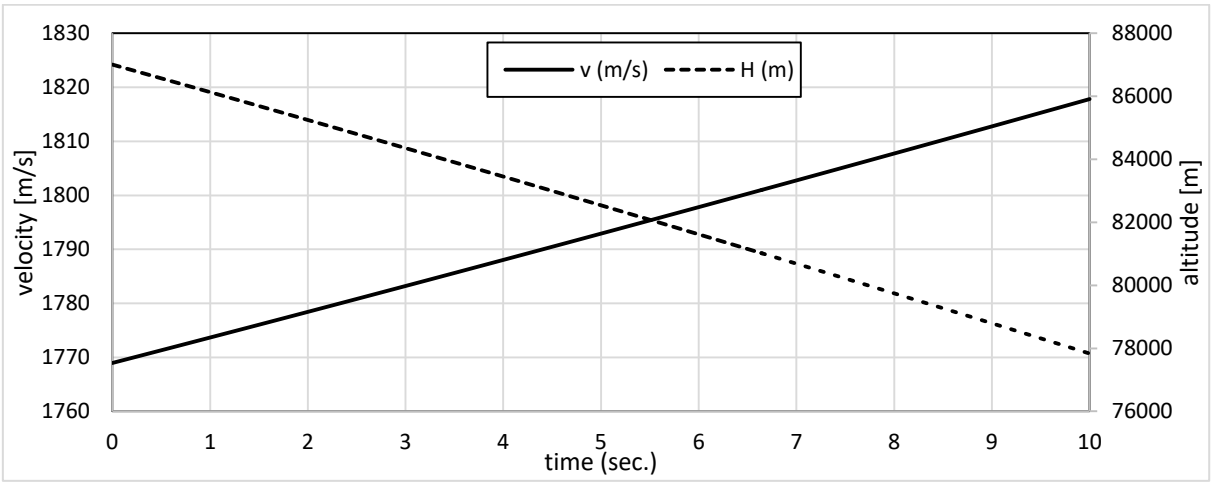

(a)

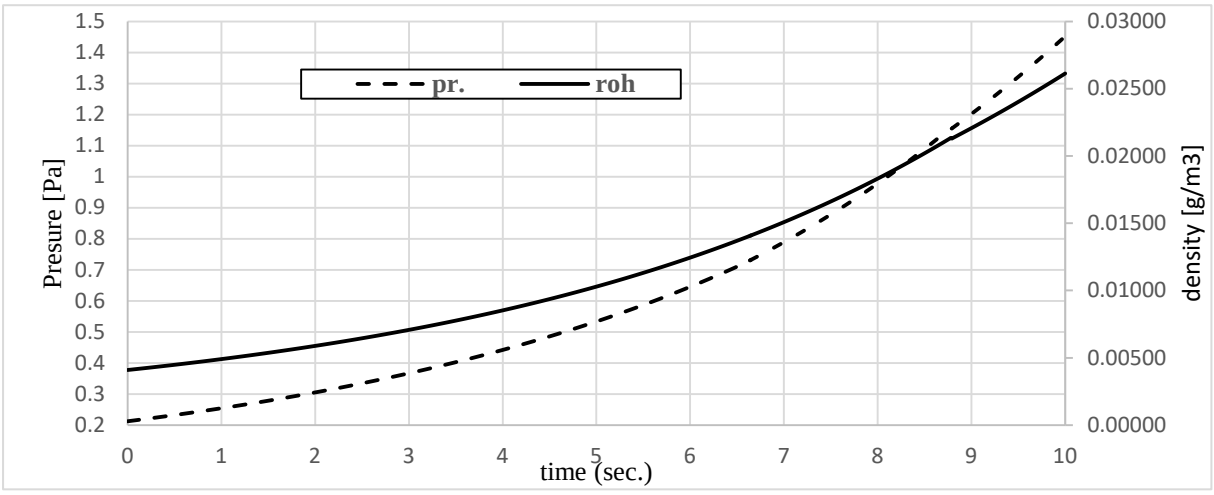

(b)

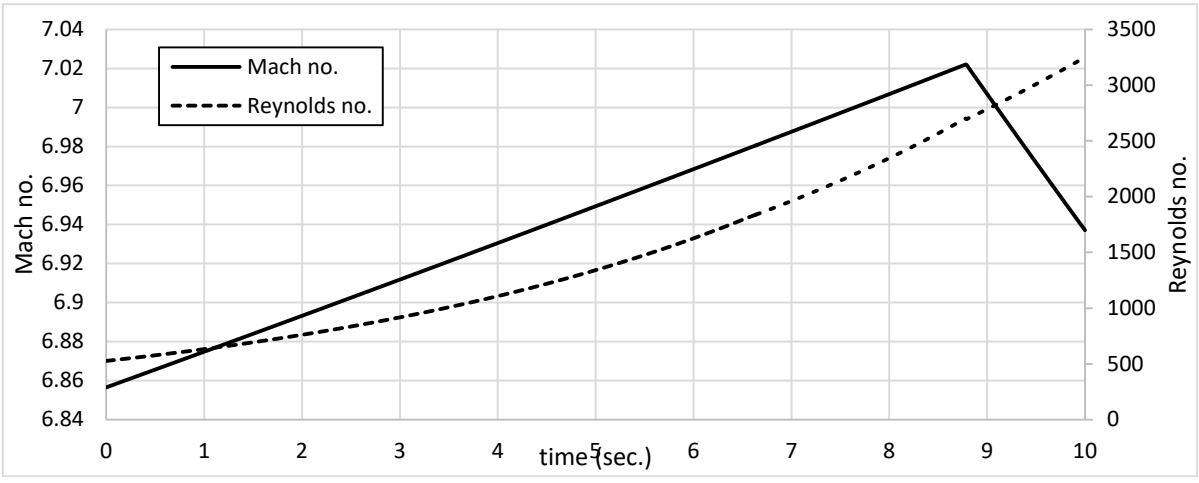

(c)

Figure 4. Temporal variation of flight conditions and freestream properties

(a) flight altitude and speed (b) atmospheric pressure and density (c) freestream Mach and Reynolds numbers

According to the flight simulation results, the freestream Mach and Reynolds number (based on vehicle base diameter) vary from 6.85 and 526 to 7.02 and 3250, respectively, in the flight zone in concern. Hence, the transient laminar density-based solver of a commercial CFD tool is utilized in the simulation [10]. The material is ideal gas with Sutherland viscosity model. The boundary conditions are pressure-far-field for the inlet with a UDFs for the gauge pressure, Mach number, and temperature while pressure-outlet boundary condition is defined at outlet. The wall thermal boundary condition is adiabatic with zero heat flux. The solution methods are implicit and flux type is Roe-FDS. For spatial discretization, a least squares cell based gradient and second order upwind for flow are applied.
In simulation, User-Defined Functions are used to simulate the variations of the freestream pressure, temperature, and Mach no. with respect to time based on trajectory simulation results.
The quality of transient simulation is dependent on its temporal resolution. To specify the proper time step size in simulation, a time step sensitivity analysis is conducted. Three time step sizes namely $0.1, 0.01, and\ 0.001$ of a second are examined to check the one that captures the phenomena occurring around the model during simulation. Freestream Mach and temperature are varied while pressure is maintained constant. Drag coefficient C_d is the parameter that is adopted as a measure. The figure below shows temporal variation of drag coefficient with different step sizes. Based on the shown results, a time step of 0.01 second is utilized.

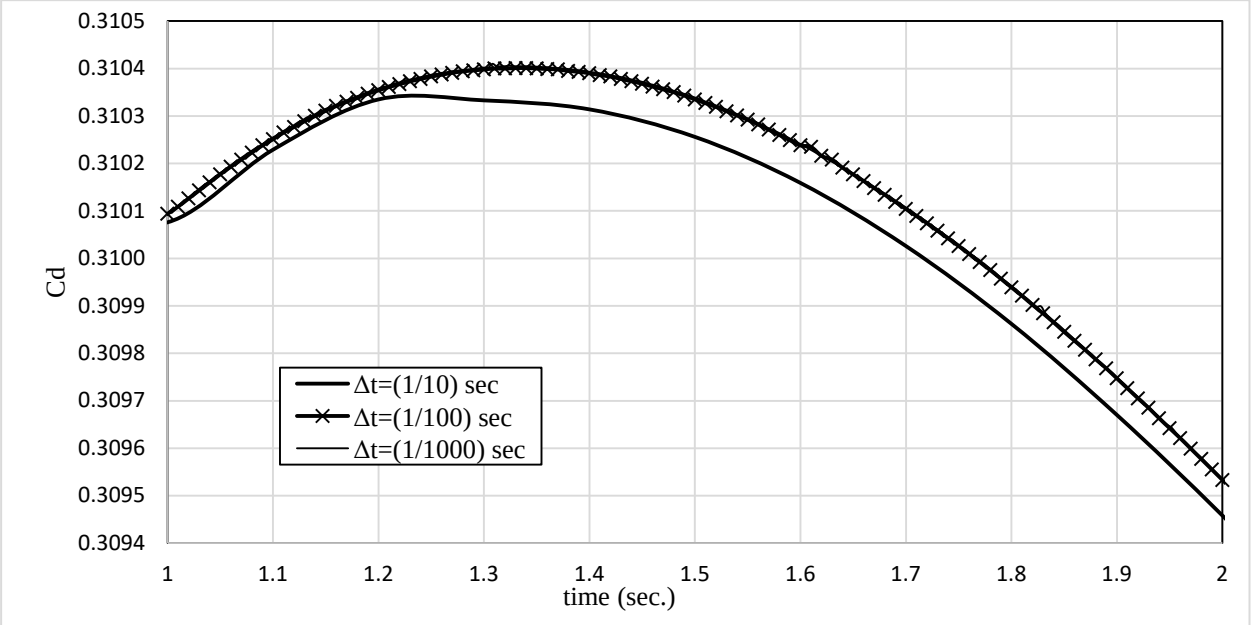

Figure 5. Results of temporal resolution analysis

3. Results and Discussion

3.1. Validation of the solver
A slender blunt bicone configuration [3] is selected to conduct the validation of the CFD solver. The configuration of the model is shown in Figure 6 below. The computational domain and solver setup have the same aspects explained earlier. Three simulation cases are undertaken at three different Mach numbers namely, 2.53, 4.0, and 5.96 to compare with the available wind tunnel results for the configuration [3]. The results of comparison are briefed in Table 2 below. The results from the CFD solver shows satisfactory agreement with wind tunnel measurements.

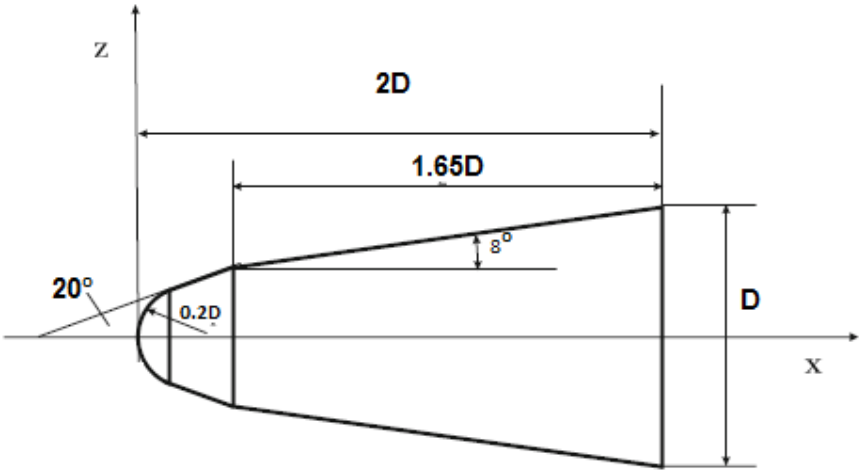

Figure 6. Configuration of the validation case

Table 2. Results of validation tests

	C_D		
Mach no.	CFD	Wind tunnel [3]	Error (%)
2.53	0.3522	0.34	3.5
4.0	0.3412	0.35	2.5
5.96	0.2237	0.23	2.7

3.2. Evolution of flow field structure during descent

The figure below shows the evolution of key flow field features at two different time instances. Pressure contours after 3 and 9 seconds from the start of simulation are shown in figure 7a whereas figure 7b illustrates the velocity contours.

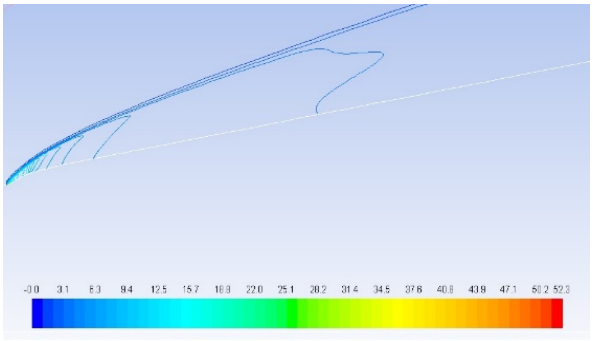

M=6.9, P=0.36 pascal, time= 3 sec.

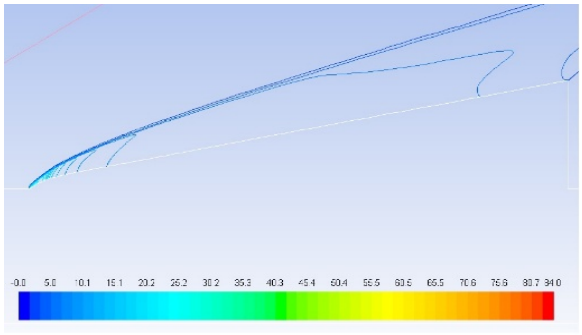

M=7, P=1.2 pascal, time= 9 sec.

(a)

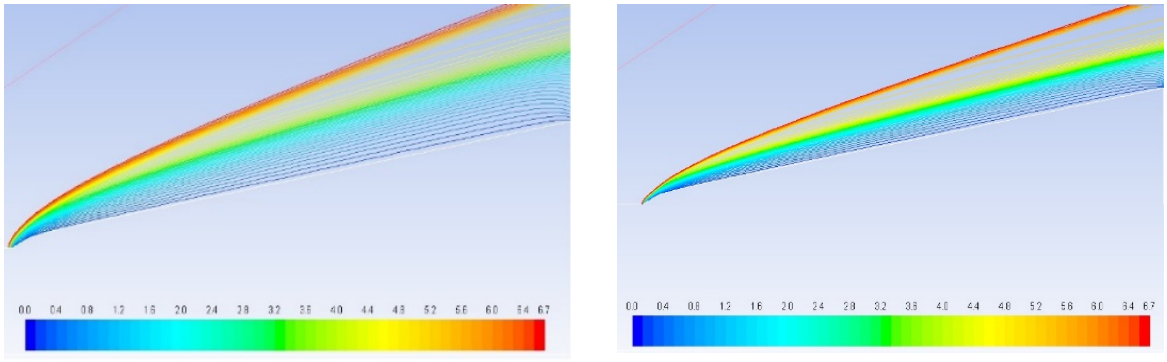

M=6.9, P=0.36 pascal, time= 3 sec. M=7, P=1.2 pascal, time= 9 sec.

(b)

Figure 7. Flowfield features at two time instances during accelerating descent

(a) pressure contours (b) Mach contours

The shock wave generated ahead of the body is oblique and straight with a small curvature at the tip. In addition, the thick boundary layer characterizing the hypersonic flow is evident. As the vehicle descends, the flight Mach number changes insignificantly (from 6.91 to 7). As a consequence, the location of shock wave with respect to the vehicles is almost unchanged. In contrast, the freestream pressure and Reynolds number at 9 seconds are, respectively, three times and six times higher than those at 3 seconds from start of simulation. Hence, the boundary layer after 9 seconds is thinner than that after 3 seconds of descent as illustrated in Fig. 7b above. Eventually, the local flow pressure and shear stress on the vehicle forebody surface vary with time as the vehicle descends as illustrated in figure 8 below.

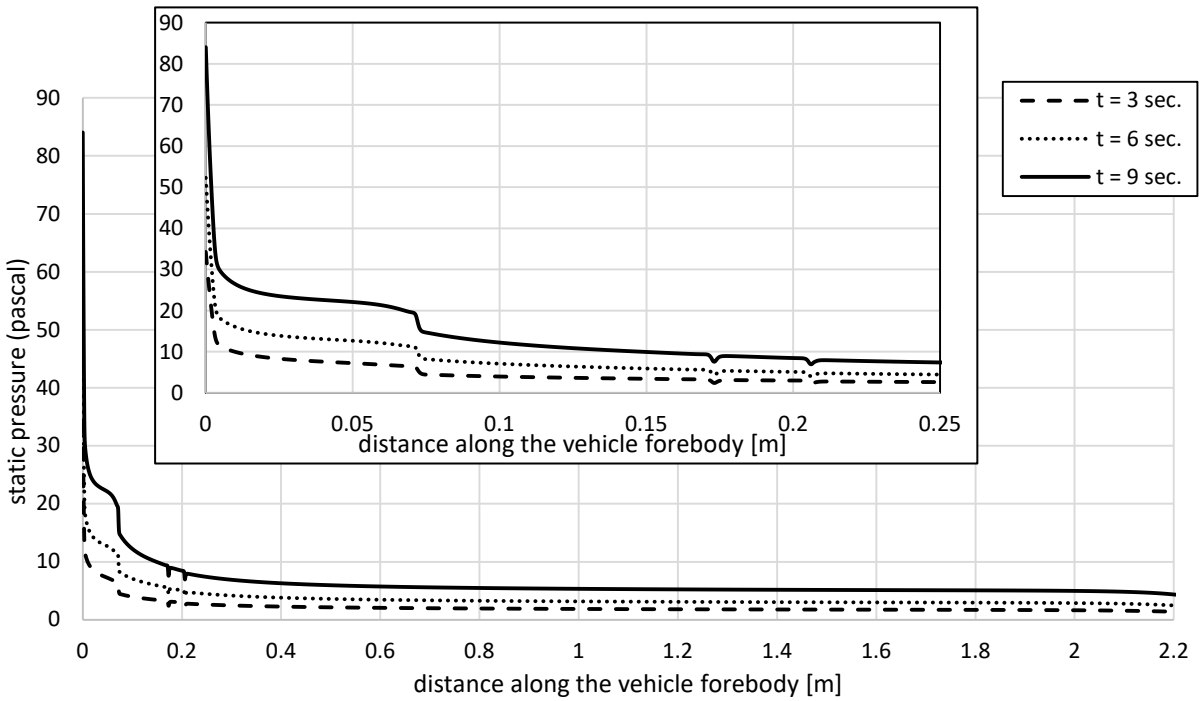

(a)

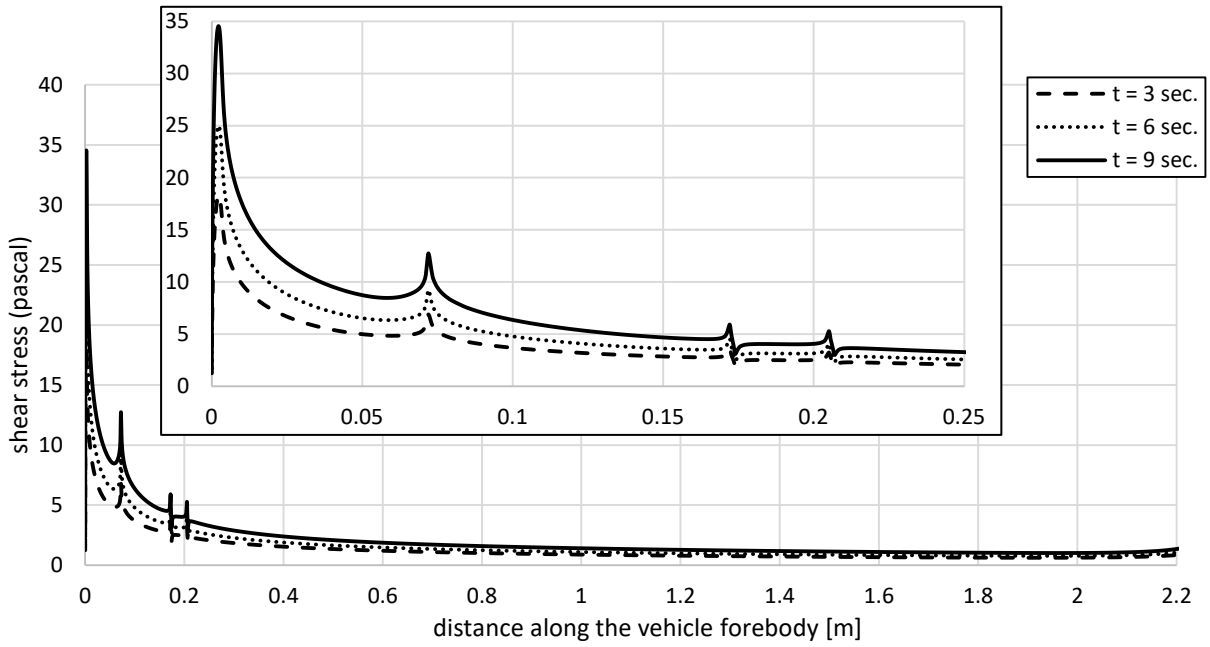

(b)

Figure 8. Variation of surface pressure and shear stress along the vehicle surface at different time instances (a) surface static flow pressure (b) surface shear stress

Over the hemispherical tip, the flow pressure drops sharply from its stagnation value. Subsequent expansions are caused by the variation in surface inclination angle with respect to the freestream. Downstream of the bi-conic tip, the flow pressure maintains nearly a constant value over the vehicle surface; this value slightly drops immediately upstream of the vehicle base. Overall, the static pressure over the vehicle surface increases as the vehicle descends. Recalling that the flow pressure downstream of the shock wave,P_2, is dependent on both freestream pressure, P_1, and Mach, M_1. This dependence is expressed as [11]:

$$P_2 = P_1\left[1 + \frac{2\gamma}{\gamma+1}(M_1^2 sin^2\beta - 1)\right] \quad (1)$$

where γ is the flow specific heat ratio, and β is the oblique shock wave angle with respect to the freestream flow direction. As the vehicle descents while accelerating, both the upstream Mach and the shock wave angle slightly change whereas the freestream pressure increases monotonically and considerably. Consequently, the vehicle surface pressure increases monotonically during descent. Finally, the thinning of the boundary layer as the vehicle descends along with the increase in flow momentum downstream of the shock wave yield the rise in surface shear stress with time.

3.3. Variation of Drag on vehicle during descent

Figure 9 below shows the temporal variation of total drag force acting on the vehicle and its coefficient during descent in the interval in concern. The drag coefficient is calculated referred to the instantaneous freestream dynamic pressure value and vehicle base area.

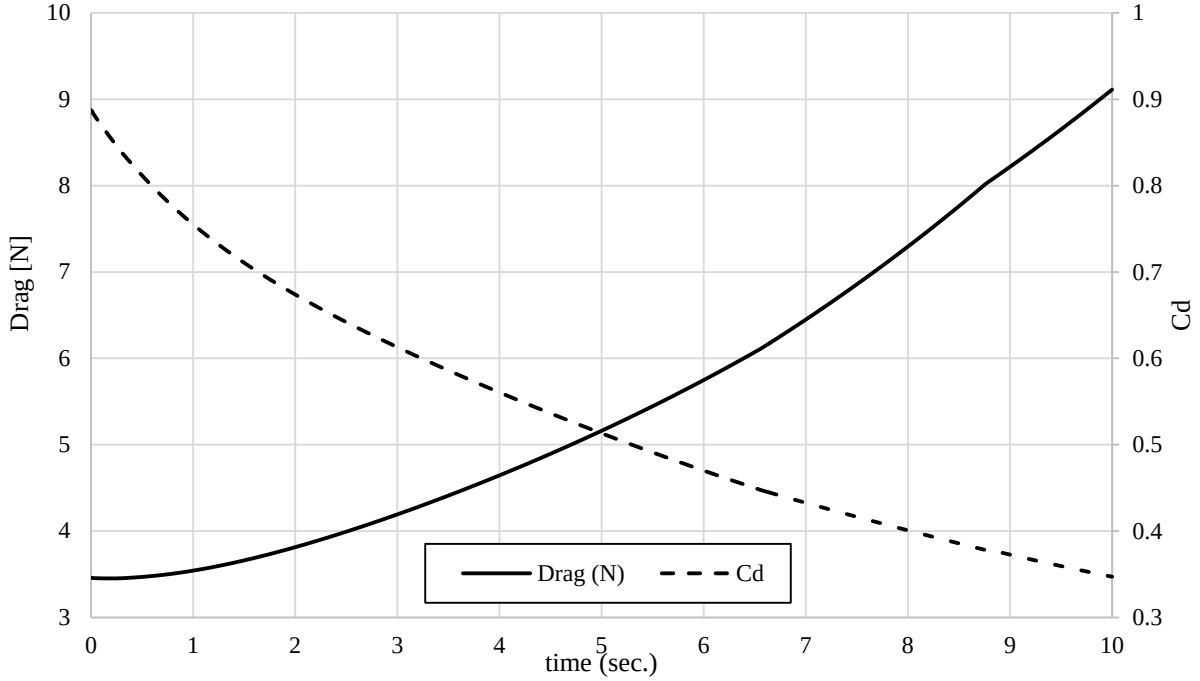

Figure 9. Temporal variation of Drag and Cd

Drag on the vehicle increases significantly with time. This is owed to the rise in both freestream speed and pressure. Table 3 below lists the components of drag on both vehicle forebody and base at three different time instances during descent.

Table 3. Instantaneous values of vehicle drag components at three time instances

				Drag [N]		
	Freestream conditions			Forebody		Base
Time	pressure [Pa]	Velocity [m/s]	Mach	Pressure drag	Friction drag	Pressure drag
3 sec.	0.366	1783.2	6.91	0.9893	3.0521	0.147
6 sec.	0.645	1797.8	6.96	1.7978	3.7975	0.146
9 sec.	1.2	1812.7	7.00	3.1589	4.9045	0.146

Drag on vehicle forebody dominates the total drag. Friction drag on forebody represents about 53% to 73% of the total drag. In addition, both pressure and friction drag increase monotonically with flight speed. In contrast, the drag coefficient decreases monotonically as the vehicle descends. Recalling that

$$C_d = \frac{D}{\frac{1}{2}\rho v^2 S_{ref}} \qquad (2)$$

As the vehicle descends, the freestream density and velocity increase with rates higher than that of the drag. This is more pronounced in the freestream velocity. Eventually, the drag coefficient decreases as the vehicle descends.

4. Conclusion

The objective of the present paper was to explore the evolution of flow field structure and temporal variation of drag acting on a reentry vehicle during accelerating descent. Focus was made on the layer of atmosphere from 87 km to 77 km through which the vehicle accelerates for ten seconds. CFD simulation of the laminar hypersonic flow was conducted. The study can be further extended by increasing the time interval of simulation, incorporating turbulent flow, and considering aerodynamic heating. The pitching reaction of the vehicle during descent can be also explored.

5. References

[1] Anderson Jr JD 2010 *Fundamentals of aerodynamics* (Tata McGraw-Hill Education)
[2] Shen C 2006 *Rarefied Gas Dynamics: Fundamentals, Simulations and Micro Flows* (Springer Science & Business Media)
[3] Celenligil M C, Moss J N, and Bird G A 1989 Direct simulation of three-dimensional flow about the AFE vehicle at high altitudes *Rarefied Gas Dynamics: Theoretical and Computational Techniques* (National Aeronautics and Space Administration) pp 447-461
[4] Weiland C 2014 *Aerodynamic data of space vehicles* (Springer Science & Business Media)
[5] Sahu J 2008 Time-accurate numerical prediction of free-flight aerodynamics of a finned projectile (Journal of Spacecraft and Rockets) pp 946-954
[6] Cayzac R, Carette E, Thepot R, and Champigny P 2005 Recent computations and validations of projectile unsteady aerodynamics *Proc. 22nd Int. Symp. on Ballistics* (Canada: Vancouver)
[7] Gledhill I M A., Forsberg k, Eliasson P, Baloyi J, and Nordstrom J 2009 Investigation of acceleration effects on missile aerodynamics using computational fluid dynamics **vol 13** (Aerospace Science and Technology) pp 197-203.
[8] *DSSC report* 2015, *DSSC-TR-2025B*
[9] *U.S. Standard Atmosphere* 1976 (Washington: U.S. Government Printing Office)
[10] *ANSYS FLUENT User guide* 2011 (ANSYS Inc.)
[11] *Equations, Tables, and Charts for Compressible Flow: Report1135* 1953 (National Advisory Committee for Aeronautics)